ACCOUNTS
of chemical research

Quantum Sized Gold Nanoclusters with Atomic Precision

HUIFENG QIAN, MANZHOU ZHU, ZHIKUN WU,
AND RONGCHAO JIN*

Department of Chemistry, Carnegie Mellon University, Pittsburgh, Pennsylvania 15213, United States

RECEIVED ON DECEMBER 22, 2011

CONSPECTUS

Gold nanoparticles typically have a metallic core, and the electronic conduction band consists of quasicontinuous energy levels (i.e. spacing $\delta \ll k_BT$, where k_BT is the thermal energy at temperature T (typically room temperature) and k_B is the Boltzmann constant). Electrons in the conduction band roam throughout the metal core, and light can collectively excite these electrons to give rise to plasmonic responses. This plasmon resonance accounts for the beautiful ruby-red color of colloidal gold first observed by Faraday back in 1857.

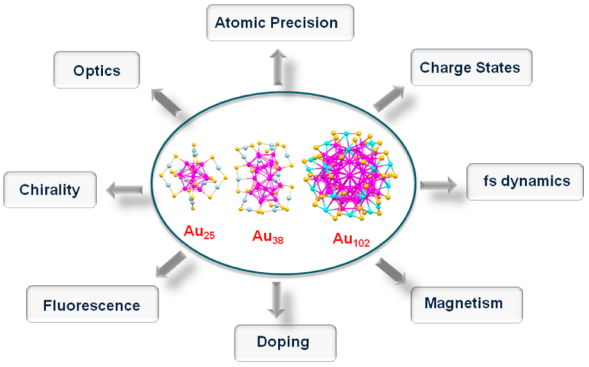

On the other hand, when gold nanoparticles become extremely small (<2 nm in diameter), significant quantization occurs to the conduction band. These quantum-sized nanoparticles constitute a new class of nanomaterial and have received much attention in recent years. To differentiate quantum-sized nanoparticles from conventional plasmonic gold nanoparticles, researchers often refer to the ultrasmall nanoparticles as nanoclusters.

In this Account, we chose several typical sizes of gold nanoclusters, including $Au_{25}(SR)_{18}$, $Au_{38}(SR)_{24}$, $Au_{102}(SR)_{44}$, and $Au_{144}(SR)_{60}$, to illustrate the novel properties of metal nanoclusters imparted by quantum size effects. In the nanocluster size regime, many of the physical and chemical properties of gold nanoparticles are fundamentally altered. Gold nanoclusters have discrete electronic energy levels as opposed to the continuous band in plasmonic nanoparticles. Quantum-sized nanoparticles also show multiple optical absorption peaks in the optical spectrum versus a single surface plasmon resonance (SPR) peak at 520 nm for spherical gold nanocrystals. Although larger nanocrystals show an fcc structure, nanoclusters often have non-fcc atomic packing structures. Nanoclusters also have unique fluorescent, chiral, and magnetic properties.

Due to the strong quantum confinement effect, adding or removing one gold atom significantly changes the structure and the electronic and optical properties of the nanocluster. Therefore, precise atomic control of nanoclusters is critically important: the nanometer precision typical of conventional nanoparticles is not sufficient. Atomically precise nanoclusters are represented by molecular formulas (e.g. $Au_n(SR)_m$ for thiolate-protected ones, where n and m denote the respective number of gold atoms and ligands).

Recently, major advances in the synthesis and structural characterization of molecular purity gold nanoclusters have made in-depth investigations of the size evolution of metal nanoclusters possible. Metal nanoclusters lie in the intermediate regime between localized atomic states and delocalized band structure in terms of electronic properties. We anticipate that future research on quantum-sized nanoclusters will stimulate broad scientific and technological interests in this special type of metal nanomaterial.

1. Introduction

Bulk gold adopts a face-centered cubic (fcc) structure, as do gold nanocrystals (e.g., above ~2 nm diameter). An interesting question is whether the fcc structure would collapse at sufficiently small size. The answer is yes. Then, the major questions are what new structure(s) ultrasmall gold nanoparticles will adopt and, accordingly, how their physicochemical properties will be altered. Research on such ultrasmall gold nanoparticles in the quantum size regime (ca. subnanometer to ~2 nm core size; often called gold nanoclusters) has been intensely pursued in recent years.[1]

Unlike large gold nanoparticles, whose optical properties are dominated by surface plasmon resonances (SPR) due to

Published on the Web 06/21/2012 www.pubs.acs.org/accounts
10.1021/ar200331z

excitation of electrons in the *continuous* conduction band, gold nanoclusters, instead, exhibit *discrete* electronic structure and molecule-like properties,[1−5] such as a HOMO−LUMO transition of a one-electron nature (in contrast with collective-electron plasmon excitation in large nanoparticles). It would be instructive to estimate at what size gold nanoparticles will exhibit distinct quantum size effects. One may use the free electron theory to estimate the quantum size regime. The average spacing (δ) of electronic energy levels roughly follows the following relation:[6]

$$\delta \approx \frac{E_f}{N} \quad (1)$$

where E_f is the Fermi energy and N is the number of gold atoms. Since N scales as d^3 (note: d is particle diameter), the spacing is thus inversely proportional to the cube of particle size. With decreasing size, the spacing δ becomes larger, and the resultant effect will be manifested in the physicochemical properties of small particles. If one uses the thermal energy (k_BT) at room temperature (~298 K) as a criterion, electronic energy quantization becomes distinct when δ is larger than k_BT.

$$\delta \geq k_BT \quad (2)$$

Substituting the Fermi energy of gold (E_f = 5.5 eV) into the equations, one obtains the critical number of gold atoms to be ~200−300 or the equivalent diameter ~1.8−2.1 nm (roughly 2 nm); note that the number of gold atoms and the particle volume are related by the following:

$$N = (59 \text{ atoms} \cdot \text{nm}^{-3}) \cdot V \text{ (nm}^3\text{)} \quad (3)$$

Thus, the ~2 nm size is that at which electronic energy quantization will become important, and below this size the collective plasmon mode will no longer be supported. Thus, the size regime for quantum-sized nanoclusters is below ~2 nm. Considering the extreme sensitivity of the properties of gold nanoclusters to the number of gold atoms in the particle, these ultrasmall particles are denoted as Au_nL_m, where n is the number of gold atoms and m is the number of ligands (such as thiolate, −SR).

In early seminal work[2,7] Whetten et al. isolated a series of narrow size distributed nanoparticles in the range of 1.0−3.5 nm by solvent fractionation. Several distinct critical sizes were observed, including species of ~5, ~8, ~14, ~22, ~28, 34−38, ~46, ~57, and ~93 kDa core mass (typically in the form of $Au_nS_m^+$, as determined by laser desorption ionization mass spectrometry, LDI-MS, k = 1000). However, true monodispersity of Au nanoparticles at the *atomic* level was not obtained at that time. For fundamental studies on the quantum size effects in metal nanoclusters, it is crucial to prepare *atomically monodisperse* nanoclusters.

Recently, significant advances have been achieved in the synthesis, crystal structure determination, and physicochemical property studies of atomically precise, gold−thiolate nanoclusters (denoted as $Au_n(SR)_m$).[1,4] A number of $Au_n(SR)_m$ nanoclusters of molecular purity have been obtained by bulk solution synthetic methods,[1] such as $Au_{25}(SR)_{18}$, $Au_{36}(SR)_{23}$, $Au_{38}(SR)_{24}$, $Au_{102}(SR)_{44}$, and $Au_{144}(SR)_{60}$ nanoclusters.[8−14] These molecular purity nanoclusters have allowed in-depth studies of the intriguing properties of quantum-sized gold nanoclusters, such as the size dependent HOMO−LUMO transition, the redox properties of the gold core, magnetism, chirality and its relation with ligands and surface gold atoms, as well as doping of Au nanoclusters with foreign atoms.

In this Account, we choose several typical sizes of gold nanoclusters, including $Au_{25}(SR)_{18}$, $Au_{38}(SR)_{24}$, $Au_{102}(SR)_{44}$, and $Au_{144}(SR)_{60}$, to illustrate the novel properties of metal nanoclusters imparted by quantum size effects. Much work still remains to be pursued in future research. We anticipate that such quantum-sized metal nanoclusters will emerge as a new class of promising nanomaterials.

2. $Au_{25}(SR)_{18}$ Nanoclusters

2.1. Atomic Monodispersity and Crystal Structure. Monodispersity is a very critical issue in the synthetic work of metal nanoclusters. If the nanocluster product is a mixture, it is very difficult to determine the exact formula of the nanocluster and to attribute any meaningful properties with it. To characterize the monodispersity of nanoclusters, mass spectrometry (MS) has become the most important and useful tool. Mass spectrometry gives the highest precision (e.g., within a fraction of one Dalton), which is critical for precisely determining the formula of nanoclusters. While transmission electron microscopy (TEM) is a powerful tool for nanomaterials, it is not very helpful in nanoclusters, as a high energy electron beam often causes severe aggregation of nanoclusters.

In early work on mass spectrometry characterization of $Au_n(SR)_m$ nanoclusters, laser desorption ionization (LDI) and matrix-assisted laser desorption ionization (MALDI) were employed. However, LDI or MALDI tended to break the Au−S and/or S−C bonds; hence, *intact* cluster mass peaks (without loss of ligands or gold atoms) were not achieved then.[7] In addition, the limited purity of nanoclusters further

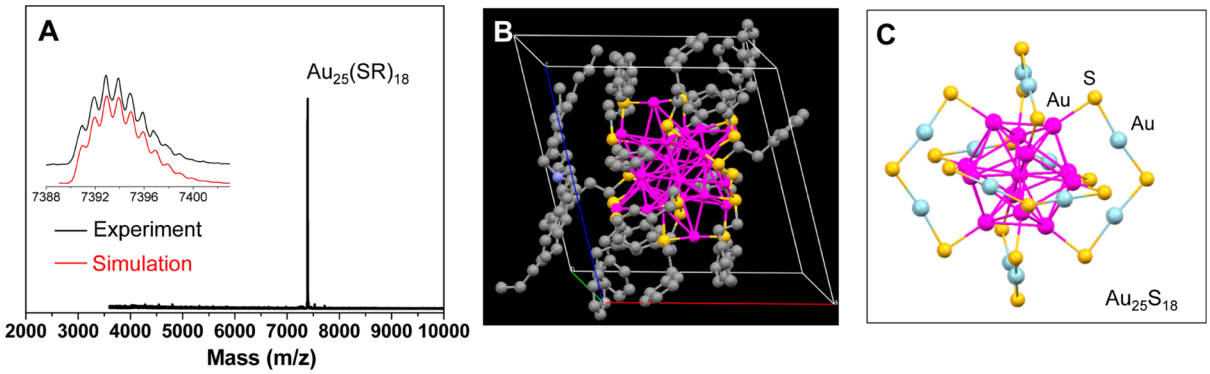

FIGURE 1. (A) Negative mode ESI-MS of $Au_{25}(SC_2H_4Ph)_{18}^{-}TOA^{+}$ (where TOA stands for tetraoctylammonium); (B) crystal structure of $Au_{25}(SC_2H_4Ph)_{18}^{-}TOA^{+}$; (C) atomic arrangement of the $Au_{25}S_{18}$ framework. Adapted with permission from ref 10.

complicated the mass spectrometric analysis. It was hard to know whether the observed broad peak came from one size or multiple sizes of nanocluster. Compared to LDI and MALDI, electrospray ionization (ESI) is a much softer ionization technique and allows the survival of intact Au cluster ions. However, early ESI-MS analysis was only amenable for aqueous samples. The Whetten group used glutathione (GSH) as ligands and prepared water-soluble Au clusters.[15] An abundant cluster species was separated by polyacrylamide gel electrophoresis (PAGE). The cluster mass was determined to be ~10.4 kDa by ESI-MS, but unfortunately the formula was erroneously assigned to $Au_{28}(SG)_{16}$ due to insufficient ESI-MS resolution then. In 2005, the Tsukuda group performed high resolution ESI-MS analysis of a series of PAGE-isolated $Au_n(SG)_m$ clusters and corrected the $Au_{28}(SG)_{16}$ formula (FW = 10415.8) as $Au_{25}(SG)_{18}$ (FW = 10437.5).[4] The two formulas merely differ by ~22 Da out of 10.4 kDa; thus, a lesson from this story is that achieving *accurate* cluster mass is very critical for correct assignment of the formula. With respect to the Au_{25} nanocluster, the Murray group reported an organic soluble species which was erroneously assigned to $Au_{38}(SCH_2CH_2Ph)_{24}$ prior to 2007[16] but later corrected as $Au_{25}(SCH_2CH_2Ph)_{18}$.[3] The three clusters were finally found to be the same one. Overall, it should be stressed that *one cannot be too careful in assigning the cluster formula*.

Obtaining molecular purity nanoclusters in the synthesis and performing careful mass spectrometry characterization (especially ESI-MS) in conjunction with other analyses are very important to correctly determine cluster formulas. With respect to the synthesis of $Au_n(SR)_m$ nanoclusters, early work suffered from the production of mixed cluster sizes; thus, the product had to be separated, for instance, by fractionation, gel electrophoresis, or chromatography.[2−4,17] As discussed above, the purity of nanoclusters is of critical importance for crystallization and studies of their new properties. Along this line, Jin and co-workers developed a kinetically controlled method for synthesizing high purity $Au_{25}(SR)_{18}$ nanoclusters in high yield.[18] An interesting "size focusing" process was discovered.[19] The as-obtained $Au_{25}(SR)_{18}$ nanoclusters showed molecular purity (Figure 1A). The size-focusing method has been demonstrated to be versatile for different thiolate ligands, including $-SC_2H_4Ph$, $-SC_{12}H_{25}$, $-SG$, and $-SC_{10}H_{22}COOH$,[19] as well as for the different-sized $Au_n(SR)_m$ nanoclusters.[1]

After the synthesis of molecular purity $Au_{25}(SCH_2CH_2Ph)_{18}$ in high yield,[18] Zhu et al. further succeeded in crystallization of $Au_{25}(SCH_2CH_2Ph)_{18}$, and the total structure of $Au_{25}(SCH_2CH_2Ph)_{18}$ was solved (Figure 1B−C);[10] of note, the Murray group independently reported the same crystal structure.[9] The $Au_{25}(SR)_{18}$ nanocluster exhibits a core−shell structure, that is, an icosahedral Au_{13} core and a Au_{12} shell consisting of six "staple-like" motifs of $-S(R)-Au-S(R)-Au-S(R)-$ (abbreviated as $Au_2(SR)_3$; Figure 1C). The $Au_{25}S_{18}$ framework adopts a quasi-D_{2h} symmetry.

2.2. Electronic Structure and Optical Absorption Properties. The available crystal structure of the Au_{25} nanocluster permitted an in-depth understanding of its electronic structure and optical absorption spectrum by performing density functional theory (DFT) calculations.[10,20] Akola et al.[21] suggested a superatom picture to account for the stability of $Au_{25}(SR)_{18}^{-}$ by assuming that each $-SR$ ligand localizes one 6s electron of gold; the nominal 8e count of $Au_{25}(SR)_{18}^{-}$ appears to conform to superatoms, but the stability of $[Au_{25}(SR)_{18}]^0$ and $[Au_{25}(SR)_{18}]^+$ (section 2.4) cannot be explained.

DFT calculations (Figure 2A) show that the HOMO of $Au_{25}(SR)_{18}$ is nearly triply degenerate, corresponding to a set of superatomic *p* orbitals delocalized in the Au_{13} core, and that the LUMO (doubly degenerate) and LUMO+1

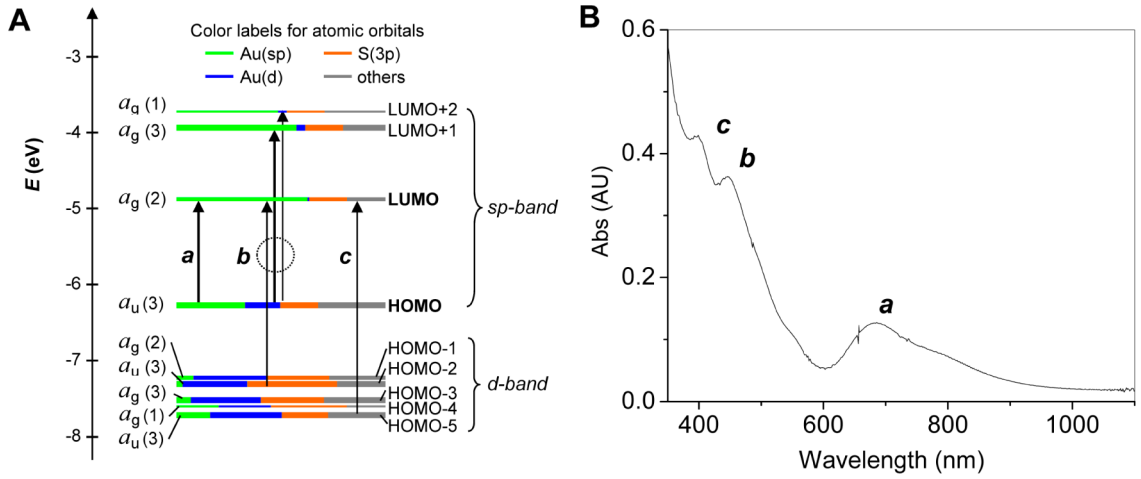

FIGURE 2. (A) Kohn–Sham orbital level diagram and (B) peak assignment for the UV–vis absorption spectrum of $[Au_{25}(SR)_{18}]^-$ nanoclusters. Adapted with permission from ref 10.

(triply degenerate) constitute the split superatomic *d* orbital.[20,21] The HOMO and lowest three LUMOs mainly contain 6*sp* orbitals of gold atoms, forming the *quantized sp* band (in contrast with the continuous *sp* band in metallic gold).[10] The HOMO–1 to HOMO–5 are mainly composed of the $5d^{10}$ atomic orbitals and form the *d* band.

The optical properties of Au nanoclusters are particularly appealing due to the quantum size effect. The absorption spectrum of $Au_{25}(SR)_{18}$ shows multiple bands at 670 nm, 450 nm, and 400 nm (Figure 2B). The calculated spectrum of $Au_{25}(SR)_{18}$ agrees well with the experimental one.[10] The electronic transition at λ = 670 nm (peak a in Figure 2B) corresponds to the LUMO ← HOMO transition (Figure 2A), which is essentially an intraband (sp ← sp) transition. The band at 450 nm (peak b) comes from the mixed intraband (sp ← sp) and interband (sp ← d) transitions. The transition at 400 nm (peak c) mainly arises from the interband (sp ← d) transition.

Overall, the molecule-like multiple absorption bands of $Au_{25}(SR)_{18}$ nanoclusters are all due to single-electron transitions between quantized electronic energy levels. This behavior is fundamentally different from the optical excitation in larger gold nanocrystals—which exhibit a distinct SPR band due to collective excitation of conduction electrons. Future work should investigate how the transition from one-electron to collective-electron excitation occurs.

2.3. Fluorescence and Ultrafast Electron Relaxation Dynamics. The fluorescence of gold nanoclusters has attracted wide research interest due to their potential application in biology and sensing. However, the exact origin of fluorescence is still not clear.[22–27] Generally, there are two possible sources of fluorescence: (i) the metal core (e.g., a manifestation of the quantum size effect) and (ii) the interactions between metal core and surface ligands. The fluorescence of $Au_{25}(SR)_{18}$ clusters (R = C_6H_{13}, C_2H_4Ph, glutathiolate, *etc.*) was found to be affected by the ligands and metal core charge state.[23] Bigioni et al. observed photoluminescence in the near-infrared region (1100–1600 nm) for 1.1 and 1.7 nm particles.[24] Wu et al. found that the surface of $Au_{25}(SR)_{18}$ played a major role in the fluorescence generation;[23] specifically, the ligands with electron rich atoms (e.g., O, N) or groups (e.g., –COOH, $-NH_2$) can considerably enhance fluorescence. The photoluminescence quantum yield of $Au_{25}(SR)_{18}$ should be further improved for practical applications (e.g., bioimaging).

The $Au_{25}(SR)_{18}$ nanoclusters also exhibit strong two-photon absorption, as reported by Ramakrishna et al.[28] Devadas et al. reported electron transfer between $Au_{25}(SR)_{18}$ nanoclusters and surface-bound dyes.[29] As for the ultrafast electron dynamics, Miller et al. reported femtosecond dynamics of anionic $Au_{25}(SR)_{18}$ clusters.[30] Their measurements show that an extremely fast (<200 fs) internal conversion process occurred between the excited states of the Au_{13} core and a 1.2 ps process was assigned to the core-to-surface relaxation. Qian et al. studied the ultrafast electron dynamics of both anionic and neutral $Au_{25}(SR)_{18}$ nanoclusters (Figure 3).[31] In both charge states, photoexcitation occurs into two nondegenerate states near the HOMO–LUMO gap that are derived from the core orbitals, indicating that the HOMO orbital set is split. A large difference in the lifetimes of the core excitations was observed, with anionic $Au_{25}(SR)_{18}$ exhibiting a decay rate more than 1000 times slower than that of the neutral cluster.[31] Clusters of both charge states show strong coupling to two different coherent phonon

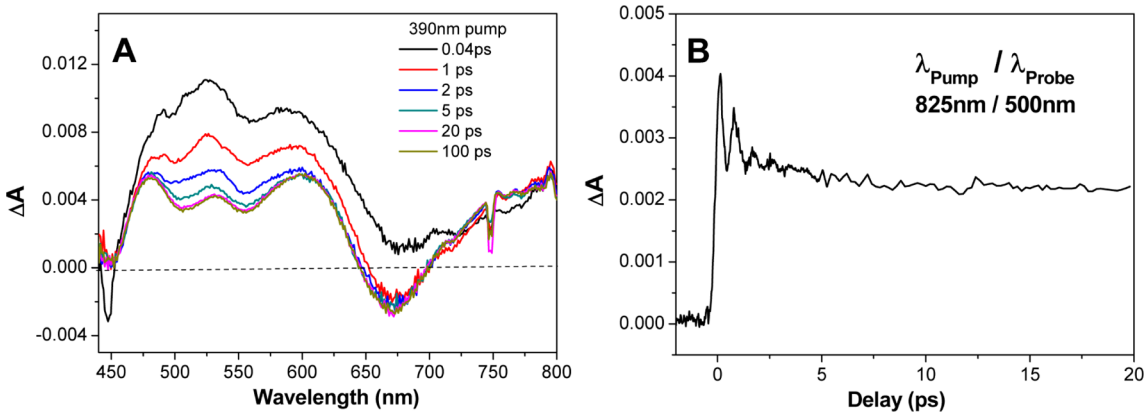

FIGURE 3. (A) Transient absorption spectra at various delay times for $[Au_{25}(SR)_{18}]^-$ and (B) a kinetic trace (825 nm pump and 500 nm probe) showing coherent phonon oscillations in the first few picoseconds. Adapted with permission from ref 31.

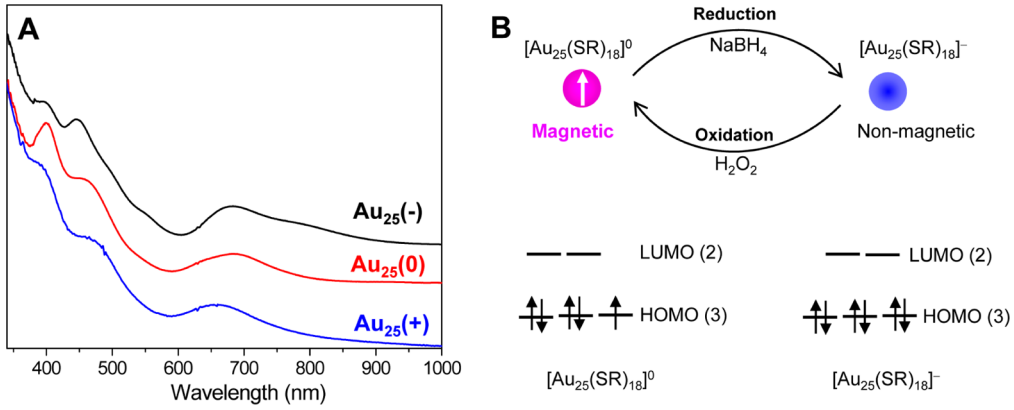

FIGURE 4. (A) UV−vis spectra of $[Au_{25}(SC_2H_4Ph)_{18}]^q$ ($q = -1, 0, +1$); (B) reversible conversion between the neutral and anionic $Au_{25}(SR)_{18}$ nanoclusters and electron energy level diagrams for the neutral and anionic clusters. Adapted with permission from refs 32 and 34.

modes, which are observed at 2.4 and 1.2 THz. The electron−phonon coupling is analyzed in terms of the spectral distribution and damping of the coherent modes.[31] The two coherent phonon modes still remain to be explained in a future effort.

2.4. Charge States and Magnetism of $[Au_{25}(SR)_{18}]^q$ ($q = -1$, 0, $+1$). The native $Au_{25}(SR)_{18}$ bears a negative charge (counterion: *n*-tetraoctylammonium cation, TOA^+). The $[Au_{25}(SR)_{18}]^-$ cluster can be readily oxidized to $[Au_{25}(SR)_{18}]^0$ and to $[Au_{25}(SR)_{18}]^+$ by chemical oxidation.[32−34] Considering the oxidation of $Au_n(SR)_m$ nanoclusters, one would speculate that the thiolate ligands should be oxidized first (which was the case in thiol-SAM on bulk gold surfaces). But the Au_{25} nanoclusters gave an unexpected result: the negative charge residing in the Au_{13} core was lost due to oxidization, rather than the thiolate ligands being oxidized (which would result in destabilization of the clusters).[32] The underlying mechanism is that the HOMO orbital of $[Au_{25}(SR)_{18}]^q$ is primarily contributed by the Au_{13} core, rather than by surface Au−SR bonds; thus, HOMO electrons (e.g., the negative charge on the cluster) are first lost in an oxidation process.

Zhu et al. solved the crystal structure of charge-neutral $Au_{25}(SR)_{18}$ and found that the $Au_{25}S_{18}$ frameworks for $q = -1$ and 0 are similar.[32] The $+1$ state should also have a similar framework according to the clues from NMR spectroscopy in recent work by the Maran group[33] and by Liu et al.[34] The charge effect is distinctly manifested in the optical spectra of $[Au_{25}(SR)_{18}]^q$ clusters. As shown in Figure 4A, the $[Au_{25}(SR)_{18}]^-$ cluster exhibits three main absorption peaks at 400, 450, and 670 nm, as well as a broad shoulder at ~800 nm. As for the $[Au_{25}(SR)_{18}]^0$ cluster, the 400 nm peak becomes more prominent while the 450 nm peak becomes less distinct; concurrently, the ~800 nm shoulder band (which is characteristic of the $[Au_{25}(SR)_{18}]^-$ cluster) disappears. As for $[Au_{25}(SR)_{18}]^+$, the 400 and 450 nm peaks both become less distinct and the lowest energy absorption peak blue shifts to ~660 nm.[33,34] These spectroscopic fingerprints allow for easy identification of the charge state of $[Au_{25}(SR)_{18}]^q$ nanoclusters.

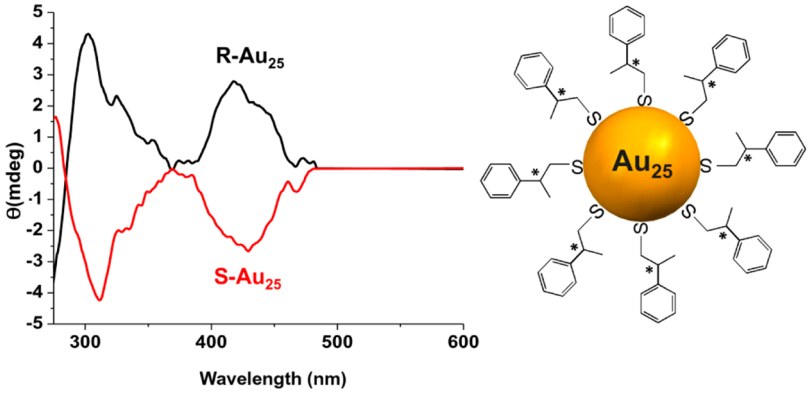

FIGURE 5. CD spectra of Au_{25} nanoclusters capped by chiral thiol ligands ($-SCH_2C^*H(CH_3)Ph$). Adapted with permission from ref 40.

Among the three charge states of $Au_{25}(SR)_{18}$, $[Au_{25}(SR)_{18}]^0$ nanoclusters were found to exhibit interesting paramagnetism originating in the itinerant electron.[32] Single gold atoms are paramagnetic due to the unpaired $6s^1$ electron, while bulk gold is diamagnetic. The evolution of magnetism from single gold atoms to nanoparticles and to bulk gold is important for fundamental science and remains to be pursued in future work. Negishi et al. reported the observation of paramagnetism in different sized $Au_n(SR)_m$ nanoclusters in their early study,[35] but the unknown structures of these clusters at that time precluded the study of the origin of magnetism. Reversible switching of paramagnetism in $[Au_{25}(SR)_{18}]^q$ was attained by controlling the charge state (Figure 4B).[32] The $[Au_{25}(SR)_{18}]^-$ and $[Au_{25}(SR)_{18}]^+$ clusters were diamagnetic.[34] The observed magnetism in $[Au_{25}(SR)_{18}]^0$ arises from an unpaired spin in its HOMO orbital, and the spin is mainly distributed in the Au_{13} core, rather than in the exterior $Au_2(SR)_3$ staples.[32] This finding is in striking contrast with the previous thought that the magnetism of gold may arise from the particle surface via charge transfer in the Au−S bonds.

2.5. Chiral $Au_{25}(SR^*)_{18}$ (SR^* = Chiral Thiolate). Chiral gold nanoparticles are attractive for enantioselective catalysis. Chirality has been found in a number of gold nanoclusters. Schaaff et al. reported that L-glutathione-protected nanoclusters showed optical circular dichroism (CD) activity.[36] Gautier et al. prepared and separated a series of CD-active gold nanoclusters with *N*-isobutyrl-L-cysteine and *N*-isobutyrl-D-cysteine.[37] Yao et al. synthesized a pair of gold nanoclusters enantiomers protected by optically active thiols: D- and L-penicillamine, which showed a mirror image in CD spectra.[38] With respected to the origin of chirality in gold nanoparticles, Schaaff et al.[36] proposed three possible mechanisms: (1) the cluster has an inherently chiral core; (2) the ligands adsorb in a chiral pattern; (3) the chiral centers in the ligand induce the optical activity in the metal core's electronic structure. For the first possibility, the reported structures of $Au_{102}(SR)_{44}$[13] and $Au_{38}(SR)_{24}$[12] indeed exhibit a chiral arrangement of surface gold atoms in these clusters.

In the case of $Au_{25}(SR)_{18}$ nanoclusters, previous research showed that the phenylethylthiolate-protected $Au_{25}(SCH_2CH_2Ph)_{18}$ has no CD activity, while glutathiolate-protected $Au_{25}(SG)_{18}$ showed distinct CD signals.[36,39] Of note, the null CD signal of $Au_{25}(SCH_2CH_2Ph)_{18}$ is not due to a racemic mixture;[40] rather, the $Au_{25}(SCH_2CH_2Ph)_{18}$ nanocluster is inherently achiral. Recently, chirally modified phenylethylthiols at the 2-position ($HSCH_2C^*H(CH_3)Ph$, abbreviated as pet* and *R*- and *S*-isomers) have been designed and used to prepare the (*R*)-$Au_{25}(pet^*)_{18}$ and (*S*)-$Au_{25}(pet^*)_{18}$ nanoclusters.[40] The $Au_{25}(pet^*)_{18}$ clusters exhibit mirror-imaged CD spectra (Figure 5). These optically active nanoclusters are close analogues of optically *nonactive* $Au_{25}(SCH_2CH_2Ph)_{18}$, whose structure has been determined by X-ray crystallography. On the basis of the atomic structure and electronic properties of well-defined Au_{25} nanoclusters, the chirality of $Au_{25}(SR^*)_{18}$ is not caused by the metal core but by the surface ligands and surface gold atoms of the cluster.[40] In theoretical work, Sanchez-Castillo et al. identified the role of the slightly distorted Au_{25} core in the optical activity and enhancement by the dissymmetric location of the ligands.[41] Further research will reveal more insight into the origin of charality in nanoclusters.

2.6. Doping of $Au_{25}(SR)_{18}$. Doping of $Au_{25}(SR)_{18}$ clusters with a foreign atom has been attained. Fields-Zinna et al. reported the observation of mono-Pd doped $Pd_1Au_{24}(SCH_2CH_2)_{18}$ mixed with $Au_{25}(SCH_2CH_2)_{18}$.[42] Negishi et al. isolated pure $Pd_1Au_{24}(SC_{12}H_{25})_{18}$ by solvent fractionation and high-performance liquid chromatography (HPLC).[43] There are three possible doping sites of Pd in the $Au_{25}(SR)_{18}$ structure: the Au_{13} core's center, the Au_{13} core's surface, and the $Au_{12}(SR)_{18}$ shell. DFT studies indicated that the site for Pd-doping is the center of the icosahedral core.[43] Qian et al.

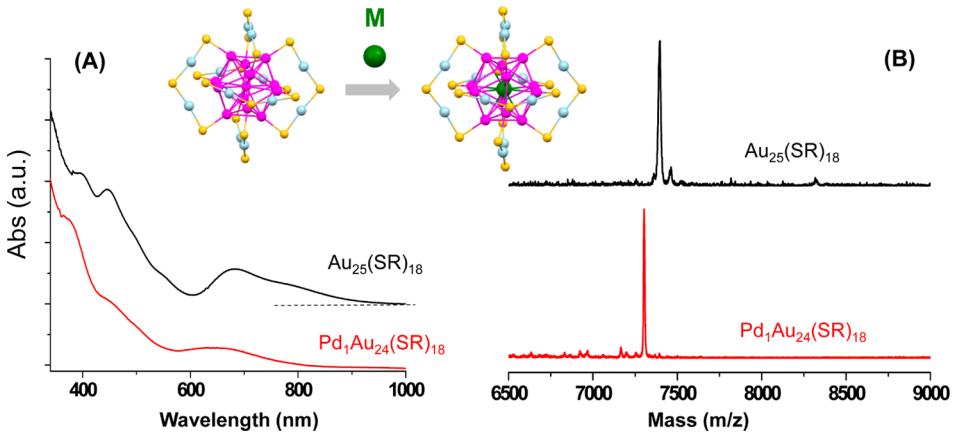

FIGURE 6. UV−vis absorption spectra (A) and MALDI-MS (B) of $Au_{25}(SR)_{18}$ (black profiles) and $Pd_1Au_{24}(SR)_{18}$ (red profiles). Adapted with permission from ref 44.

reported two methods to synthesize and isolate $Pd_1Au_{24}(SCH_2CH_2Ph)_{18}$ nanoclusters (Figure 6), and the centrally doped $Pd_1Au_{24}(SR)_{18}$ structure was identified by its fragmentation pattern in mass spectra.[44] The isolated $Pd_1Au_{24}(SCH_2CH_2Ph)_{18}$ clusters show a somewhat different absorption spectrum from that of $Au_{25}(SCH_2CH_2Ph)_{18}$ (Figure 6A).[43,44]

Other than Pd, Jiang et al. predicted that 14 elements from groups 1, 2, and 10−14 can replace the central gold atom of $Au_{25}(SR)_{18}$ while maintaining the geometric structure.[45] For example, DFT calculations indicated that the magnetic dopings of $Au_{25}(SR)_{18}$ with Mn, Cr, and Fe are all thermodynamically favorable.[46] Future synthetic work may reveal more information about magnetically doped nanoclusters.

3. Other $Au_n(SR)_m$ Nanoclusters

While tremendous work on $Au_{25}(SR)_{18}$ has been done, other sizes of gold nanoclusters have not been pursued as extensively as $Au_{25}(SR)_{18}$. Below we choose $Au_{38}(SR)_{24}$, $Au_{102}(SR)_{44}$, and $Au_{144}(SR)_{60}$ and briefly summarize some key results that have been obtained.

$Au_{38}(SR)_{24}$ Nanoclusters. The synthesis and structure of Au_{38} nanoclusters have been attained.[12,47−50] After the $Au_{38}(SR)_{24}$ formula in early reports[16] was corrected as $Au_{25}(SR)_{18}$,[4] some researchers questioned whether $Au_{38}(SR)_{24}$ really existed. Shortly, Chaki et al. reported the isolation of alkanethiolate-protected Au_{38} nanoclusters, and the $Au_{38}(SC_nH_{2n+1})_{24}$ formula was unequivocally determined by ESI-MS analysis.[48] Toikkanen et al. synthesized hexanethiolate-protected Au_{38} clusters.[49] The $Au_{38}(SC_nH_{2n+1})_{24}$ synthesis by Chaki et al. involved a complicated process of solvent extraction for isolation of Au_{38}, and the yield was quite low. Qian et al. developed a two-step method to synthesize $Au_{38}(SCH_2CH_2Ph)_{24}$ and attained a yield of ~25%.[50] In the first step, a mixture of glutathione-protected $Au_n(SG)_m$ ($38 \leq n \leq 100$) was prepared in acetone solution. In the second step, excess thiol ($PhCH_2CH_2SH$) was added to effect ligand exchange (SG to SCH_2CH_2Ph) on the Au clusters and subsequent conversion of the Au cluster mixture to monodisperse $Au_{38}(SCH_2CH_2Ph)_{24}$.[50] ESI-MS indicated molecular purity of as-prepared $Au_{38}(SCH_2CH_2Ph)_{24}$ nanoclusters (Figure 7A). The UV−vis absorption spectrum of $Au_{38}(SR)_{24}$ exhibited distinct peaks at 1050, 750, 620, 560, 520, and 490 nm (Figure 7B).[50] The high yielding synthesis of molecular purity $Au_{38}(SCH_2CH_2Ph)_{24}$ clusters has led to successful crystallization and structure determination.[12] Surprisingly, the unit cell of $Au_{38}(SR)_{24}$ crystals contains a pair of enantiomeric nanoclusters (*R*- and *L*-handedness; Figure 7C). Each isomer contains a face-sharing biicosahedral Au_{23} core and a $Au_{15}(SR)_{24}$ shell. The $Au_{15}(SR)_{24}$ shell consists of three $Au(SR)_2$ (monomeric staples) and six $Au_2(SR)_3$ (dimeric staples). The chirality of the cluster arises from the dual-propeller-like distribution of the six $Au_2(SR)_3$ staples, giving rise to two enantiomers.[12] MacDonald et al. recently reported solution phase X-ray spectroscopic studies on $Au_{38}(SR)_{24}$ nanoclusters.[51] Doping of $Au_{38}(SR)_{24}$ by Pd and Ag has also been reported.[52,53]

$Au_{102}(SR)_{44}$ Nanoclusters. With respect to the $Au_{102}(p\text{-MBA})_{44}$ nanocluster (where *p*-MBA stands for *p*-mercaptobenzoic acid), Jadzinsky et al. reported its total structure in 2007, which was indeed the first structure reported for thiolate-capped gold nanoclusters (Figure 8).[13] The work first revealed the RS−Au−SR bonding mode (so-called "staple" motif) on the surface of gold nanoclusters, in striking contrast to the standard model that was thought before, in which the thiol group was directly attached to a close-packed gold substrate. The $Au_{102}(p\text{-MBA})_{44}$ possesses a core

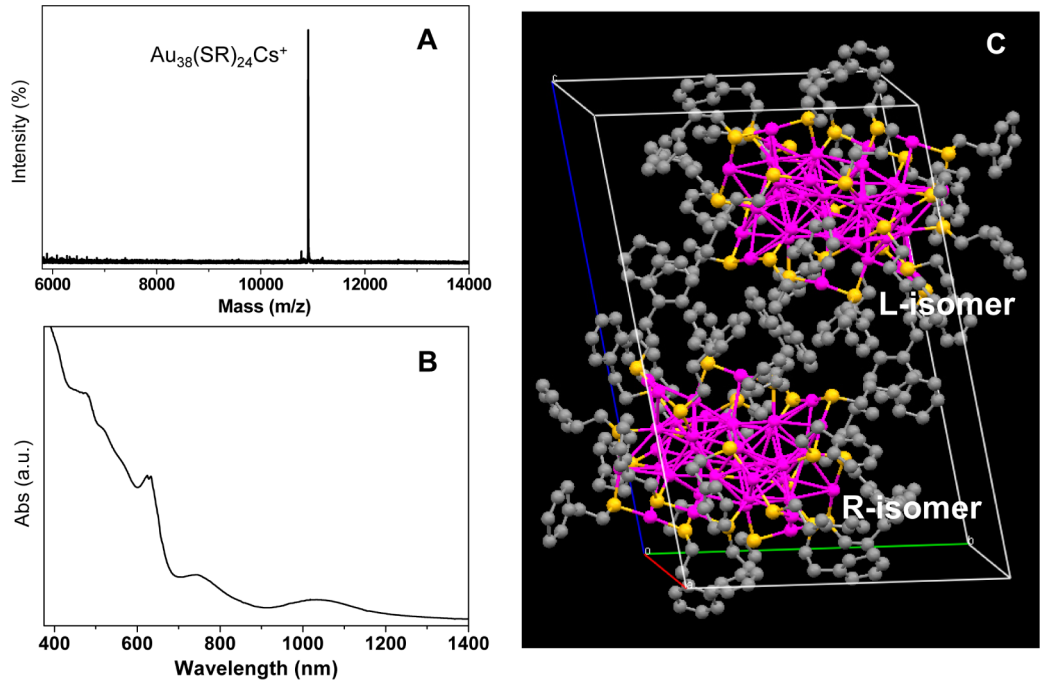

FIGURE 7. ESI mass spectrum (A), UV−vis spectrum (B), and crystal structure (C) of $Au_{38}(SC_2H_4Ph)_{24}$ nanoclusters. Adapted with permission from refs 12 and 50.

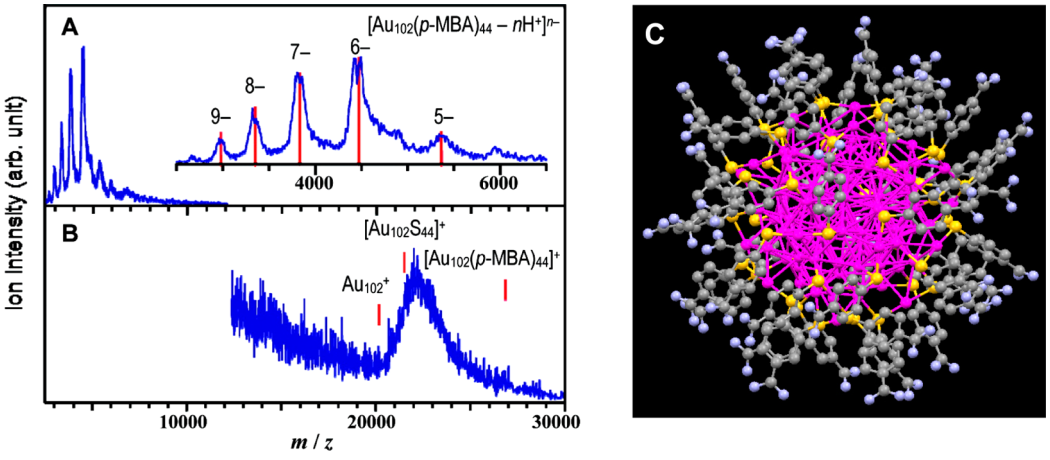

FIGURE 8. (A) ESI-MS, (B) MALDI-MS, and (C) crystal structure of $Au_{102}(p\text{-MBA})_{44}$ nanoclusters. Adapted with permission from refs 13 and 57.

of Au_{79} and a shell of $Au_{23}(p\text{-MBA})_{44}$. The $Au_{23}(p\text{-MBA})_{44}$ shell is composed of 19 $Au(SR)_2$ staples and two $Au_2(SR)_3$ staples.[13] The $Au_{102}(p\text{-MBA})_{44}$ exhibits chirality arising from the arrangement of the equatorial gold atoms and associated thiolates on the surface.[13] The $Au_{102}(SR)_{44}$ structure provided a model system for theoretical studies.[54−56] The stability of this nanocluster was explained by the closure of 58 free valence electrons (i.e., 102 − 44 = 58 e), and the calculated HOMO−LUMO gap of Au_{102} (~0.5 eV) is in agreement with experiment.[55,57]

$Au_{144}(SR)_{60}$ Nanoclusters. Another well-defined nanocluster is $Au_{144}(SR)_{60}$. Chaki et al.[48] prepared Au clusters of core mass 29 kDa and determined the formula to be $Au_{144}(SC_nH_{2n+1})_{59}$ by ESI-MS. Qian et al. developed a two-step method to prepare monodisperse Au_{144} nanoclusters, and the formula was determined to be $Au_{144}(SR)_{60}$.[14] The one-ligand discrepancy is perhaps due to the oxidation treatment in the work of Chaki et al. to impart charges to the cluster in their ESI-MS analysis. Qian used metal ion (Cs^+) adduction to $Au_{144}(SR)_{60}$ clusters in ESI-MS analysis.[14] An ambient synthesis of $Au_{144}(SR)_{60}$ in methanol has also been developed,[58] which is versatile for different thiolate ligands, and the yield of $Au_{144}(SR)_{60}$ is 10−20% (Au atom basis). The crystal structure of Au_{144} remains to be determined in future efforts.

Prospects for the Future. The field of quantum-sized metal nanoclusters has just started to flourish. Much work remains to be pursued in the future. Quantum-sized metal nanoclusters lie in between isolated metal atoms and the bulk form. Such nanoclusters exhibit many unique properties; for example, the one-electron transition picture in nanoclusters is in striking contrast with the collective-electron excitation (i.e., surface plasmon resonance) in metallic Au nanoparticles. Understanding the fundamental properties, in particular the evolution of metal nanoclusters with size, is one of the grand challenges in the field. A prerequisite is to synthesize a series of metal nanoclusters ranging from about a dozen to a few hundred atoms with precise size control. For the atomic structures of nanoclusters, every size comes as a surprise; this is indeed the most exciting part of nanocluster research. Crystallization of nanoclusters is still a major challenge; on the other hand, theoretical predictions of structures have been demonstrated.[21,47] The total structures of nanoclusters are the basis of understanding their electronic, optical, and other physicochemical properties. The development of metallic behavior in metal nanoclusters with increasing size will reveal how the surface plasmon resonance comes into being in sufficiently large clusters.

Another major issue is to understand what determines the stability of $Au_n(SR)_m$ nanoclusters with strict stoichiometries (n, m). No theory has been able to predict stable (n, m) stoichiometries. The two general arguments prevalent in the literature—electron shell closing and atomic shell closing—appear insufficient for ligand-capped nanoclusters, although these arguments work well for gas phase bare clusters. In future work, experimental work (e.g., solving the crystal structures of different sized nanoclusters) and theoretical input (e.g., electronic structure evaluations) are expect to reveal the fundamental principles that govern the stability of gold nanoclusters protected by thiolate, including dithiolate.[59] The $Au_n(SR)_m$ nanoclusters have shown promise in catalysis[60] and other fields. Overall, future research on quantum-sized nanoclusters is anticipated to stimulate long-lasting scientific and technological interests in this special type of metal nanoparticles.

We acknowledge research support by the Air Force Office of Scientific Research under AFOSR Award No. FA9550-11-1-9999 (FA9550-11-1-0147) and the Camille Dreyfus Teacher–Scholar Awards Program.

BIOGRAPHICAL INFORMATION

Huifeng Qian is a graduate student in the Jin group at Carnegie Mellon University. He obtained both his B.S. in Chemistry (2004) and his M.S. in Materials Science (2007) from Shanghai Jiao Tong University, China. His research interests are semiconductor quantum dots and noble metal nanoclusters.

Manzhou Zhu was a postdoctoral researcher in the Jin group and is now Professor of Chemistry at Anhui University (China). He received his Ph.D. in Chemistry from the University of Science and Technology of China (USTC) in 2000. His research interests focus on photoinduced electron transfer, chemosensors, and nanomaterials.

Zhikun Wu was a postdoctoral researcher in the Jin group and is now a Professor at the Institute of Solid State Physics, Chinese Academy of Science. His research interests are nanoparticles and molecular materials.

Rongchao Jin is an Associate Professor of Chemistry at Carnegie Mellon University. He received his B.S. in Chemical Physics from USTC in 1995, his M.S. in Physical Chemistry/Catalysis from Dalian Institute of Chemical Physics in 1998, and his Ph.D. in Chemistry from Northwestern University in 2003. After three years of postdoctoral research at the University of Chicago, he joined the chemistry faculty of Carnegie Mellon University in 2006. His current research interests focus on atomically precise noble metal nanoparticles.

FOOTNOTES

*To whom correspondence should be addressed. E-mail: rongchao@andrew.cmu.edu.
The authors declare no competing financial interest.

REFERENCES

1 Jin, R.; Qian, H.; Wu, Z.; Zhu, Y.; Zhu, M.; Mohanty, A.; Garg, N. Size Focusing: A Methodology for Synthesizing Atomically Precise Gold Nanoclusters. *J. Phys. Chem. Lett.* **2010**, *1*, 2903–2910.

2 Schaaff, T. G.; Shafigullin, M. N.; Khoury, J. T.; Vezmar, I.; Whetten, R. L.; Cullen, W. G.; First, P. N.; Gutierrez-Wing, C.; Ascensio, J.; Jose-Yacaman, M. J. Isolation of Smaller Nanocrystal Au Molecules: Robust Quantum Effects in Optical Spectra. *J. Phys. Chem. B* **1997**, *101*, 7885–7891.

3 Parker, J. F.; Fields-Zinna, C. A.; Murray, R. W. The Story of a Monodisperse Gold Nanoparticle: $Au_{25}L_{18}$. *Acc. Chem. Res.* **2010**, *43*, 1289–1296.

4 Negishi, Y.; Nobusada, K.; Tsukuda, T. Glutathione-Protected Gold Clusters Revisited: Bridging the Gap between Gold(I)-Thiolate Complexes and Thiolate-Protected Gold Nanocrystals. *J. Am. Chem. Soc.* **2005**, *127*, 5261–5270.

5 Pettibone, J. M.; Hudgens, J. W. Synthetic Approach for Tunable, Size-Selective Formation of Monodisperse, Diphosphine-Protected Gold Nanoclusters. *J. Phys. Chem. Lett.* **2010**, *1*, 2536–2540.

6 Kubo, R.; Kawabata, A.; Kobayashi, S. Electronic-Properties of Small Particles. *Annu. Rev. Mater. Sci.* **1984**, *14*, 49–66.

7 Whetten, R. L.; Khoury, J. T.; Alvarez, M. M.; Murthy, S.; Vezmar, I.; Wang, Z. L.; Stephens, P. W.; Cleveland, C. L.; Luedtke, W. D.; Landman, U. Nanocrystal Gold Molecules. *Adv. Mater.* **1996**, *8*, 428–433.

8 Shichibu, Y.; Negishi, Y.; Tsukuda, T.; Teranishi, T. Large-Scale Synthesis of Thiolated Au_{25} Clusters via Ligand Exchange Reactions of Phosphine-Stabilized Au_{11} Clusters. *J. Am. Chem. Soc.* **2005**, *127*, 13464–13465.

9 Heaven, M. W.; Dass, A.; White, P. S.; Holt, K. M.; Murray, R. W. Crystal Structure of the Gold Nanoparticle $[N(C_8H_{17})_4][Au_{25}(SCH_2CH_2Ph)_{18}]$. *J. Am. Chem. Soc.* **2008**, *130*, 3754–3755.

10 Zhu, M.; Aikens, C. M.; Hollander, F. J.; Schatz, G. C.; Jin, R. Correlating the Crystal Structure of A Thiol-Protected Au_{25} Cluster and Optical Properties. *J. Am. Chem. Soc.* **2008**, *130*, 5883–5885.

11 Nimmala, P. R.; Dass, A. $Au_{36}(SPh)_{23}$ Nanomolecules. *J. Am. Chem. Soc.* **2011**, *133*, 9175–9177.

12 Qian, H.; Eckenhoff, W. T.; Zhu, Y.; Pintauer, T.; Jin, R. Total Structure Determination of Thiolate-Protected Au_{38} Nanoparticles. *J. Am. Chem. Soc.* **2010**, *132*, 8280–8281.

13 Jadzinsky, P. D.; Calero, G.; Ackerson, C. J.; Bushnell, D. A.; Kornberg, R. D. Structure of a Thiol Monolayer-Protected Gold Nanoparticle at 1.1 Å Resolution. *Science* **2007**, *318*, 430–433.

14 Qian, H.; Jin, R. Controlling Nanoparticles with Atomic Precision: The Case of $Au_{144}(SCH_2CH_2Ph)_{60}$. *Nano Lett.* **2009**, *9*, 4083–4087.

15 Schaaff, T. G.; Knight, G.; Shafigullin, M. N.; Borkman, R. F.; Whetten, R. L. Isolation and Selected Properties of a 10.4 kDa Gold: Glutathione Cluster Compound. *J. Phys. Chem. B* **1998**, *102*, 10643–10646.

16 Donkers, R. L.; Lee, D.; Murray, R. W. Synthesis and Isolation of the Molecule-like Cluster $Au_{38}(PhCH_2CH_2S)_{24}$. *Langmuir* **2004**, *20*, 1945–1952.

17 Tsunoyama, H.; Negishi, Y.; Tsukuda, T. Chromatographic Isolation of "Missing" Au_{55} Clusters Protected by Alkanethiolates. *J. Am. Chem. Soc.* **2006**, *128*, 6036–6037.

18 Zhu, M.; Lanni, E.; Garg, N.; Bier, M. E.; Jin, R. Kinetically Controlled, High-yield Synthesis of Au_{25} Clusters. *J. Am. Chem. Soc.* **2008**, *130*, 1138–1139.

19 Wu, Z.; Suhan, J.; Jin, R. One-Pot Synthesis of Atomically Monodisperse, Thiol-Functionalized Au_{25} Nanoclusters. *J. Mater. Chem.* **2009**, *19*, 622–626.

20 Aikens, C. M. Electronic Structure of Ligand-Passivated Gold and Silver Nanoclusters. *J. Phys. Chem. Lett.* **2011**, *2*, 99–104.

21 Akola, J.; Walter, M.; Whetten, R. L.; Häkkinen, H.; Grönbeck, H. On the Structure of Thiolate-Protected Au_{25}. *J. Am. Chem. Soc.* **2008**, *130*, 3756–3757.

22 Zheng, J.; Petty, J. T.; Dickson, R. M. High Quantum Yield Blue Emission from Water-Soluble Au_8 Nanodots. *J. Am. Chem. Soc.* **2003**, *125*, 7780–7781.

23 Wu, Z.; Jin, R. On the Ligand Role in the Fluorescence of Gold Nanoclusters. *Nano Lett.* **2010**, *10*, 2568–2573.

24 Bigioni, T. P.; Whetten, R. L.; Dag, O. Near-Infrared Luminescence from Small Gold Nanocrystals. *J. Phys. Chem. B* **2000**, *104*, 6983–6986.

25 Wang, G.; Huang, T.; Murray, R. W.; Menard, L.; Nuzzo, R. G. Near-IR Luminescence of Monolayer-Protected Metal Clusters. *J. Am. Chem. Soc.* **2005**, *127*, 812–813.

26 Chaudhari, K.; Xavier, P. L.; Pradeep, T. Understanding the Evolution of Luminescent Gold Quantum Clusters in Protein Templates. *ACS Nano* **2011**, *5*, 8816–8827.

27 Shibu, E. S.; Muhammed, M. A. H.; Tsukuda, T.; Pradeep, T. Ligand Exchange of $Au_{25}SG_{18}$ Leading to Functionalized Gold Clusters: Spectroscopy, Kinetics, and Luminescence. *J. Phys. Chem. C* **2008**, *112*, 12168–12176.

28 Ramakrishna, G.; Varnavski, O.; Kim, J.; Lee, D.; Goodson, T. Quantum-Sized Gold Clusters as Efficient Two-Photon Absorbers. *J. Am. Chem. Soc.* **2008**, *130*, 5032–5033.

29 Devadas, M. S.; Kwak, K.; Park, J.-W.; Choi, J.-H.; Jun, C.-H.; Sinn, E.; Ramakrishna, G.; Lee, D. Directional Electron Transfer in Chromophore-Labeled Quantum-Sized Au_{25} Clusters: Au_{25} as an Electron Donor. *J. Phys. Chem. Lett.* **2010**, *1*, 1497–1503.

30 Miller, S. A.; Womick, J. M.; Parker, J. F.; Murray, R. W.; Moran, A. M. Femtosecond Relaxation Dynamics of $Au_{25}L_{18}^-$ Monolayer-Protected Clusters. *J. Phys. Chem. C* **2009**, *113*, 9440–9444.

31 Qian, H.; Sfeir, Y.; Jin, M.; Ultrafast, R. Relaxation Dynamics of $[Au_{25}(SR)_{18}]^q$ Nanoclusters: Effects of Charge State. *J. Phys. Chem. C* **2010**, *114*, 19935–19940.

32 Zhu, M.; Aikens, C. M.; Hendrich, M. P.; Gupta, R.; Qian, H.; Schatz, G. C.; Jin, R. Reversible Switching of Magnetism in Thiolate-Protected Au_{25} Superatoms. *J. Am. Chem. Soc.* **2009**, *131*, 2490–2492.

33 Venzo, A.; Antonello, S.; Gascon, J. A.; Guryanov, I.; Leapman, R. D.; Perera, N. V.; Sousa, A. A.; Zamuner, M.; Zanella, A.; Maran, F. Effect of the Charge State ($z = -1, 0, +1$) on the Nuclear Magnetic Resonance of Monodisperse $Au_{25}[S(CH_2)_2Ph]_{18}^z$ Clusters. *Anal. Chem.* **2011**, *83*, 6355–6362.

34 Liu, Z.; Zhu, M.-Z.; Meng, X.; Xu, G.; Jin, R. Electron Transfer between $[Au_{25}(SC_2H_4Ph)_{18}]^-TOA^+$ and Oxoammonium Cations. *J. Phys. Chem. Lett.* **2011**, *2*, 2104–2109.

35 Negishi, Y.; Tsunoyama, H.; Suzuki, M.; Kawamura, N.; Matsushita, M. M.; Maruyama, K.; Sugawara, T.; Yokoyama, T.; Tsukuda, T. X-ray magnetic circular dichroism of size-selected, thiolated gold clusters. *J. Am. Chem. Soc.* **2006**, *128*, 12034–12035.

36 Schaaff, T. G.; Whetten, R. L. Giant Gold-Glutathione Cluster Compounds: Intense Optical Activity in Metal-Based Transitions. *J. Phys. Chem. B* **2000**, *104*, 2630–2641.

37 Gautier, C.; Burgi, T. Chiral N-Isobutyryl-cysteine Protected Gold Nanoparticles: Preparation, Size Selection, and Optical Activity in the UV-vis and Infrared. *J. Am. Chem. Soc.* **2006**, *128*, 11079–11087.

38 Yao, H.; Miki, K.; Nishida, N.; Sasaki, A.; Kimura, K. Large Optical Activity of Gold Nanocluster Enantiomers Induced by a Pair of Optically Active Penicillamines. *J. Am. Chem. Soc.* **2005**, *127*, 15536–15543.

39 Wu, Z.; Gayathri, C.; Gil, R. R.; Jin, R. Probing the Structure and Charge State of Glutathione-Capped $Au_{25}(SG)_{18}$ Clusters by NMR and Mass Spectrometry. *J. Am. Chem. Soc.* **2009**, *131*, 6535–6542.

40 Zhu, M.; Qian, H.; Meng, X.; Jin, S.; Wu, Z.; Jin, R. Chiral Au_{25} Nanospheres and Nanorods: Synthesis and Insight into the Origin of Chirality. *Nano Lett.* **2011**, *11*, 3963–3969.

41 Sanchez-Castillo, A.; Noguez, C.; Garzon, I. L. On the Origin of the Optical Activity Displayed by Chiral-Ligand-Protected Metallic Nanoclusters. *J. Am. Chem. Soc.* **2010**, *132*, 1504–1505.

42 Fields-Zinna, C. A.; Crowe, M. C.; Dass, A.; Weaver, J. E. F.; Murray, R. W. Mass Spectrometry of Small Bimetal Monolayer-Protected Clusters. *Langmuir* **2009**, *25*, 7704–7710.

43 Negishi, Y.; Kurashige, W.; Niihori, Y.; Iwasa, T.; Nobusada, K. Isolation, structure, and stability of a dodecanethiolate-protected Pd_1Au_{24} cluster. *Phys. Chem. Chem. Phys.* **2010**, *12*, 6219–6225.

44 Qian, H.; Barry, E.; Zhu, Y.; Jin, R. Doping 25-Atom and 38-Atom Gold Nanoclusters with Palladium. *Acta Phys.—Chim. Sin.* **2011**, *27*, 513–519.

45 Jiang, D.; Dai, S. From Superatomic $Au_{25}(SR)_{18}$ to Superatomic $M@Au_{24}(SR)_{18}$ Shell Clusters. *Inorg. Chem.* **2009**, *48*, 2720–2722.

46 Jiang, D.; Whetten, R. L. Magnetic Doping of a Thiolated-Gold Superatom: First-Principles Density Functional Theory Calculations. *Phys. Rev. B* **2009**, *80*, No. 115402.

47 Pei, Y.; Gao, Y.; Zeng, X. C. Structural Prediction of Thiolate-Protected Au_{38}: A Face-Fused Bi-icosahedral Au Core. *J. Am. Chem. Soc.* **2008**, *130*, 7830–7832.

48 Chaki, N. K.; Negishi, Y.; Tsunoyama, H.; Shichibu, Y.; Tsukuda, T. Ubiquitous 8 and 29 kDa Gold:Alkanethiolate Cluster Compounds: Mass-Spectrometric Determination of Molecular Formulas and Structural Implications. *J. Am. Chem. Soc.* **2008**, *130*, 8608–8610.

49 Toikkanen, O.; Ruiz, V.; Ronholm, G.; Kalkkinen, N.; Liljeroth, P.; Quinn, B. M. Synthesis and Stability of Monolayer-Protected Au_{38} Clusters. *J. Am. Chem. Soc.* **2008**, *130*, 11049–11055.

50 Qian, H.; Zhu, Y.; Jin, R. Size-Focusing Synthesis, Optical and Electrochemical Properties of Monodisperse $Au_{38}(SC_2H_4Ph)_{24}$ Nanoclusters. *ACS Nano* **2009**, *3*, 3795–3803.

51 MacDonald, M.; Zhang, P.; Chen, N.; Qian, H.; Jin, R. Solution-Phase Structure and Bonding of $Au_{38}(SR)_{24}$ Nanoclusters from X-ray Absorption Spectroscopy. *J. Phys. Chem. C* **2011**, *115*, 65–69.

52 Negishi, Y.; Igarashi, K.; Munakata, K.; Ohgakea, W.; Nobusada, K. Palladium doping of magic gold cluster $Au_{38}(SC_2H_4Ph)_{24}$: formation of $Pd_2Au_{36}(SC_2H_4Ph)_{24}$ with higher stability than $Au_{38}(SC_2H_4Ph)_{24}$. *Chem. Commun.* **2012**, *48*, 660–662.

53 Kumara, C.; Dass, A. AuAg alloy nanomolecules with 38 metal atoms. *Nanoscale* **2012**, DOI: 10.1039/C2NR11781A.

54 Gao, Y.; Shao, N.; Zeng, X. C. Ab Initio Study of Thiolate-Protected Au_{102} Nanocluster. *ACS Nano* **2008**, *2*, 1497–1503.

55 Hulkko, E.; Lopez-Acevedo, O.; Koivisto, J.; Levi-Kalisman, Y.; Kornberg, R. D.; Pettersson, M.; Hakkinen, H. Electronic and Vibrational Signatures of the Au_{102}(p-MBA)$_{44}$ Cluster. *J. Am. Chem. Soc.* **2011**, *133*, 3752–3755.

56 Han, Y.-K.; Kim, H.; Jung, J.; Choi, Y. C. Understanding the Magic Nature of Ligand-Protected Gold Nanoparticle $Au_{102}(MBA)_{44}$. *J. Phys. Chem. C* **2010**, *114*, 7548–7552.

57 Levi-Kalisman, Y.; Jadzinsky, P. D.; Kalisman, N.; Tsunoyama, H.; Tsukuda, T.; Bushnell, D. A.; Kornberg, R. D. Synthesis and Characterization of Au_{102}(p-MBA)$_{44}$ Nanoparticles. *J. Am. Chem. Soc.* **2011**, *133*, 2976–2983.

58 Qian, H.; Jin, R. Ambient Synthesis of $Au_{144}(SR)_{60}$ Nanoclusters in Methanol. *Chem. Mater.* **2011**, *23*, 2209–2217.

59 Tang, Z.; Xu, B.; Wu, B.; Germann, M. W.; Wang, G. Synthesis and Structural Determination of Multidentate 2,3-Dithiol-Stabilized Au Clusters. *J. Am. Chem. Soc.* **2010**, *132*, 3367–3374.

60 Zhu, Y.; Qian, H.; Jin, R. Catalysis Opportunities of Atomically Precise Gold Nanoclusters. *J. Mater. Chem.* **2011**, *21*, 6793–6799.